Title:
FATCAT: (an efficient) Functional And Tractographic Connectivity Analysis Toolbox

Authors:
Paul A. Taylor[1,2], Ziad S. Saad[3]

[1] African Institute for Mathematical Sciences, Muizenberg, Western Cape, South Africa
[2] Department of Radiology, UMDNJ-New Jersey Medical School, Newark, NJ, USA
[3] Scientific and Statistical Computing Core, National Institutes of Health, Bethesda, MD, USA

CONFLICTS OF INTEREST: The authors declare no competing financial interests.

Running header: "Introduction to FATCAT"

Keywords: tractography; FMRI; diffusion tensor imaging (DTI); connectivity; resting state networks; amplitude of low frequency fluctuations; regional homogeneity; uncertainty estimation.

Author email addresses:
PAT: neon.taylor@gmail.com
ZSS: saadz@mail.nih.gov

Please send correspondence to:
Paul Taylor
African Institute for Mathematical Sciences
6 Melrose Road
Muizenberg 7945
Cape Town
SOUTH AFRICA

Tel: +27 (0)21 787 9320
Fax: +27 (0)21 787 9321
Email: neon.taylor@gmail.com

ABBREVIATIONS:

FATCAT: Functional And Tractographic Connectivity Analysis Toolbox
FMRI: functional magnetic resonance imaging
DTI: diffusion tensor imaging
LFF: low frequency fluctuations
ALFF: amplitude of low frequency fluctuations
fALFF: fractional amplitude of low frequency fluctuations
RSFA: resting state functional activity
FA: fractional anisotropy
MD: mean diffusivity
RD: radial diffusivity
DT: diffusion tensor
ReHo: regional homogeneity
WM: white matter
GM: gray matter
FC: functional connectivity
ROI: region of interest
DWI: diffusion-weighted imaging
ICA: independent component analysis
RSFC: resting state functional connectivity
RSN: resting state network
BOLD: blood oxygen-level dependent
FACT: fiber assessment by continuous tracking
FACTID: FACT including diagonals
TB-: task based-
RS-: resting state-
FCP: Functional Connectome Project
SEM: structural equation modeling
VAR: vector autoregressive
SVAR: structural vector auto-regressive
DCM: dynamic causal modelling
sLDSf: switching linear dynamic system for fMRI
HARDI: high angular resolution diffusion imaging
DSI: diffusion spectrum imaging
ODF: orientation distribution functions
SNR: signal-to-noise ratio

ABSTRACT:

We present a suite of software tools for facilitating the combination of FMRI and diffusion-based tractography from a network-focused point of view. The programs have been designed for investigating functionally-derived GM networks and related structural WM networks. The software comprises the Functional And Tractographic Connectivity Analysis Toolbox (FATCAT), now freely distributed with AFNI. This toolbox supports common file formats and has been designed to integrate as easily as possible with existing standard FMRI pipelines and diffusion software, such as AFNI, FSL and TrackVis. The programs are efficient, run by commandline for facilitating group processing and produce several visualizable outputs. Here, we present the programs and their underlying methods, and we also provide a test example of resting state FMRI analysis combined with tractography. Tractography results are compared with existing methods, showing significantly reduced runtime and generally similar connectivity, but with important differences such as more circumscribed tract regions and a more physiologically identifiable paths produced between several ROI pairs. Currently, FATCAT uses only DT-based tractography (one direction per voxel), but higher order models will soon be included.

1. INTRODUCTION

Over the past decade, brain connectivity has been studied in several contexts across neuroimaging modalities, using a wide array of tools for both qualitative and quantitative investigation. Functional MRI (FMRI) [Ogawa et al., 1990; Kwong et al., 1992] has been used successfully to determine the location and extent of distinct brain regions that are organized into networks for performing cognitive functions. In functional connectivity, both task-based (TB-) and resting state (RS-) FMRI have been used to identify and model interactions within regions forming several gray matter (GM) networks in the brain. RS-FMRI in particular permits the examination of several networks from a single scan session [Biswal et al., 1995; Lowe et al., 1998; Xiong et al., 1999]. In contrast, diffusion-weighted (DW) imaging methods have allowed for the characterization of local white matter (WM) properties based on how anatomical structures affect the random motion of molecules [Basser et al., 1994; Basser, 1995; Le Bihan 1995]. Using this information, tractographic techniques have reproduced several major pathways of WM architecture such as the corpus callosum, cingulate fibers, corona radiata, etc. [Mori et al., 1999; Conturo et al., 1999; Basser et al., 2000; Catani et al., 2002; Hagmann et al., 2003].

While both modalities have been used to elucidate neural differences between healthy controls and various cases of pathology, anatomical and functional data are often examined in separation, even though functional organization is linked to the anatomical one and vice versa [Simoyan and Ludlow, 2011]. More recently the emphasis on combining these complementary notions of connectivity has grown [Staempfli et al. 2008; Jbadbi & Johansen-Berg, 2011; Le Bihan & Johansen-Berg 2012], with the goal of providing a better insight into the organization and function of the brain.

Here, we present a suite of software tools for facilitating the combination of FMRI and diffusion-based tractography, called the Functional And Tractographic Connectivity Analysis Toolbox (FATCAT). The point of these tools is to assist in studying both functional networks and their associated WM pathways with the regions of interest (ROIs) forming each network delineated, to the greatest degree possible, by each individual's own data. Succinctly, the tools allow for the delineation of GM ROIs from common FMRI parameters, such as correlation, general linear modeling or independent component analysis. An efficient probabilistic tractography algorithm then identifies likely WM regions connecting these GM ROIs, and produces summary properties of these WM regions.derived from the diffusion weighted images.

We discuss the methodology of the tools, highlighting technical and novel aspects. Human data sets are used to demonstrate how the various components of FATCAT can be used for associating functional with structural connectivity measures. This toolbox was designed to integrate as easily as possible with existing standard FMRI and diffusion imaging software such as AFNI, FSL and TrackVis [Cox, 1996; Smith et al., 2004; Wang et al., 2007]. FATCAT is now freely available in

the AFNI distribution along with demo data.

The organization of this paper is as follows. In Sec. 2, typical FMRI and DTI processing procedures and parameters are briefly reviewed. In Sec. 3, the major components of the toolbox are described, emphasizing both the general purpose of each as well as technical details of calculation. In Sec. 4, examples of FATCAT usage and implementation are given for human data sets; tractographic methods in particular are emphasized. Finally, in Sec. 5, the general uses of FATCAT are discussed, along with potential developments for future versions, including higher-order diffusion models for tractography.

2. BACKGROUND

We first present a brief background of standard FMRI and DTI methodologies, focusing on the quantities often calculated in each for analysis and comparison. Much more expansive reviews can be found, e.g., [Huettel et al. 2009; Kingsley 2006; Le Bihan & Johansen-Berg 2012]. Then, we show how the features of FATCAT may be used to efficiently combine the complementary measures of FMRI and tractography. In keeping with AFNI's design, FATCAT provides mechanisms of processing, with a wide range of application and no single, prescribed pipeline. Users will need to determine how to best combine the tools for the purposes of testing their hypotheses, depending on experimental design, acquired data, overall study goals, etc. While we present FATCAT for approaches that were considered to be most common, its design allows for a great deal of flexibility and generality in use.

FMRI and associated quantities

As one goal of FMRI studies is to examine functional activation and/ or connectivity (FC) across the brain, with the underlying neuronal firing of interest mediated via the blood oxygenation level dependent (BOLD) response that is actually measured. Traditional TB-FMRI studies identify regions that exhibit a significant BOLD response to a specific stimulus and model their interactions. Alternatively, patterns of BOLD temporal fluctuations across the brain can be studied in the absence of a designated task during RS-FMRI studies. RS-FMRI allows for the concurrent study of several networks based on inter-regional covariance in low frequency fluctuation (LFF) around the range of 0.01-0.1 Hz. Commonly studied resting state networks (RSNs) include the sensorimotor, visual, default mode and executive control networks [Beckmann et al., 2005; Damoiseaux et al., 2006; Raichle et al., 2001; Seeley et al., 2007].

From TB-FMRI a variety of inter-regional functional connectivity measures can be derived such as with structural equation modeling (SEM) [McIntosh and Gonzalez-Lima, 1994], vector autoregressive (VAR) modeling [Goebel et al., 2003], structural vector auto-regressive (SVAR) analysis [Chen et al, 2011], psychophysiological interactions (PPI) [Friston et al., 1997], dynamic causal modelling (DCM) [Friston et al., 2003], switching linear dynamic system for

fMRI (sLDSf) [Smith et al., 2011]. While the models underlying these varied approaches differ considerably, the result is a measure of connectedness between regions. In RS-FMRI studies, a common approach is to use the standard (Pearson) correlation coefficient as a proxy for connectivity between regions after accounting for a variety of nuisance sources. Another approach uses independent component analysis (ICA), which estimates (spatially or temporally) independent maps [McKeown et al., 1998; Calhoun et al., 2002; Kiviniemi et al., 2003]. Spatial ICA (SICA) produces several independent component (IC) spatial maps of Z-scores of correspondence to a representative time series for each component. As might be expected, each of the aforementioned methods offers advantages and certain disadvantages in analysis, and even a minor exposition is beyond the scope of this paper. Insofar as the toolbox is concerned, these functional measures represent features of a set of GM ROIs that are to be associated with candidate WM regions that can reasonably be connecting them anatomically, and the choice of FMRI analysis is essentially independent of the tractography.

In addition to the tractography tools, several FMRI regional parameters can be estimated with programs within FATCAT, predominantly for resting state studies. While not connectivity measures per se, these measures have been found useful in describing resting state functional connectivity (RSFC). For example, ReHo (regional homogeneity, another term for the previously known Kendall's coefficient of concordance, KCC [Kendall & Babington Smith, 1939]) can be calculated from the processed time series [Zang et al., 2004]. This parameter quantifies the similarity of a time series in groups of neighboring voxels or ROIs. Other descriptors of resting state networks (RSNs) in studies of healthy controls and pathological cases include: ALFF (the amplitude of LFFs) [Zang et al., 2007], which is sum of LFF spectral amplitudes of the Fourier-transformed time series; fALFF (the fractional ALFF), in which the ALFF is scaled by the sum of the time series' amplitudes across the full spectrum [Zou et al., 2008]; and RSFA (resting state functional activity), the standard deviation of the LFF-filtered time series [Kannurpatti & Biswal, 2008].

DTI, associated quantities and tractography

As with FMRI, several categories of DW scanning exist, encompassing different levels of structural information, model assumptions, reliability and power. In all cases the relative magnitude of diffusion along a given orientation is used to gauge the amount of local structure hindering the journey of hydrogen in water.

DTI utilizes the simplest framework, in which the local diffusion properties are represented by a diffusion tensor (DT), D, having six independent elements. Due to the model assumptions of a positive, semi-definite tensor, D corresponds to the surface of an ellipsoid aligned along the greatest orientation of diffusion in a voxel. At the cost of more DW scans and greater DW-magnitude, higher order models such as high angular resolution diffusion imaging (HARDI), Q-ball imaging, diffusion spectrum imaging (DSI), orientation distribution functions (ODFs), and

others, have the advantage of being able to characterize several dominant directions of diffusion [Tuch et al., 2002; Tuch, 2004; Wedeen et al., 2005; Anderson, 2005; Ozarslan et al., 2006]. In the current version of FATCAT, only DTI-based tractography (i.e., one main diffusion direction per voxel) is supported, although multi-directional transport is planned for the next release.

In DTI, the number of DW measures along distinct gradients is typically in a range of M=20-30 with a few repetitions of the reference, non-DW measure, and sometimes 2-3 repetitions of a gradient sequence are performed to increase the signal to noise ratio (SNR). From these several standard parameters of interest may be calculated to characterize important features of the diffusion ellipsoid. The orientation and magnitude of the ellipsoid's semiaxes are respectively characterized by the DT's three, mutually orthogonal eigenvectors and the three eigenvalues. Thus, the first eigenvector, $\mathbf{e}_1$, provides the spatial orientation of the major diffusion direction, whose magnitude is characterized by the first eigenvalue, L1 (by convention, eigenvalues appear in descending order). The average diffusivity in the plane perpendicular to $\mathbf{e}_1$ is given by the radial diffusivity, RD=(L2+L3)/2, the average of the second and third eigenvalues. The relative shape of the ellipsoid is generally quantified by the fractional anisotropy (FA), a normalized standard deviation of the eigenvalues ranging between between 0 for isotropy (spherical diffusion) and 1 for maximal anisotropy (elongated diffusion). The mean diffusivity, MD=(L1+L2+L3)/3, relates to the size of the ellipsoid.

In the simplest interpretation, ellipsoids of high FA characterize voxels with major, underlying tract bundles, along which $\mathbf{e}_1$ is aligned. RD may then characterize the relative amounts of cross-structure. Tractography algorithms make use of such associations to estimate the locations of extended structures across many voxels. For deterministic tractography, seed points start in voxels above a threshold FA value and then propagate (using, for example, the local first eigenvector, Euler integration of vector fields or trajectory deflecting schemes [Basser et al., 2000; Conturo et al., 1999; Mori et al. 1999; Lazar et al., 2003; Weinstein et al., 1999; Westin et al., 1999]) until a stop criterion is reached. Tracts passing through selected ROIs of interest are stored, along with their voxel locations. With probabilistic tractography, the variances of FA and $\mathbf{e}_1$ estimates are taken into account, and many iterations of whole brain tractography are run with voxel parameters perturbed at each instance according to estimated parameter uncertainties. The resulting maps show likely locations of WM connecting the target ROIs. In FATCAT, both deterministic and probabilistic tractography utilize the FACTID algorithm, an efficient form of streamline tractography validated in a series of tests on both human data and a standard phantom [Taylor et al., 2012].

3. DESIGN AND METHODS OF FATCAT

A schematic diagram showing stages for combining FMRI (dark gray boxes) and DW-tractographic (lighter gray boxes) analyses is shown in Fig. 1. The functional data may be either TB or RS, with steps specifically for processing the latter shown with dashed lines. Dot-dashed

lines show alternate side-analyses for the DW data. The roles for the main tools in FATCAT are highlighted (bold, blue text), and general steps to be performed with existing software are given, as well (italic text). For example, the first set of steps after acquiring either FMRI or DW data typically involves some pipeline of "preprocessing." This may include motion correction and registration of volumes, spatial smoothing and despiking (or censoring) of "bad" data points, among other steps.

Functional processing

Standard goals for functional processing include, but are not limited to, localizing regions of activity, quantifying local properties and measuring connective properties among networks of these ROIs. All of these objectives are realizable for both TB- and RS-FMRI using tools in FATCAT, though we note that several of the calculable ROI-based quantities have typically been used more commonly for the latter studies. In terms of localizing functional ROIs and defining targets for tractography, however, both TB- and RS-FMRI data sets are commensurately useful.

3dRSFC is a program for estimating a variety of common RSFC parameters: ALFF, fALFF, RSFA and fRSFA (a quantity introduced here, the RSFA scaled by the standard deviation of the pre-LFF filtered time series). Since parameters such as fALFF and fRSFA are drawn from both the LFF and unfiltered series, one must be sure that the spectral features of both are calculated after identical processing. 3dRSFC also combines preprocessing features of AFNI's 3dBandpass (e.g., detrending, regressing, despiking, filtering and spatial smoothing) with parameter estimation to ensure that both LFF and unfiltered time series have analogous processing for comparisons of spectral amplitude. The outputs of this program are a data set of fully processed LFF time series and associated wholebrain maps of RSFC parameters.

3dMatch takes two sets of volumes and pairs them in a manner that maximizes the match between volume singletons. This may be used to associate and order ICA results from an individual with those of a standard reference set, since ICA results are unordered, in general. For two sets A and B, similarity is weighted towards higher intensity voxels with match being estimated as the correlation of volumes $A'=\text{sign}(A)*A^2$ with $B'=\text{sign}(B)*B^2$. There are options to set ceiling and floor values for the volumes, and one may output Dice coefficients of comparison [Dice, 1945] between masks of thresholded volumes, as well.

3dReHo computes regional homogeneity (Kendall's coefficient of concordance) on a voxelwise or on a regionwise basis. In the voxelwise case, neighborhoods may be selected around each individual voxel (i.e., neighborhoods of 6, 19 or 27), or may be formed from extended spheroidal and ellipsoidal shapes; the latter may be useful in particular in the case of anisotropic voxel dimensions. The ReHo parameter has been used in both TB- and RS-FMRI studies [Zang et al., 2004; He et al., 2007]. Additionally, the Friedman chi-square of the coefficient is estimated.

3dROIMaker is used to parcellate wholebrain FC maps of statistical measures into distinct GM networks by thresholding and spatial clustering. Individual ROIs are labeled with distinct integers, which can be made uniform across a group by supplying an approximate reference map. ROIs can be thresholded by volume to suppress clusters formed by chance (for example, using 3dClustSim in AFNI). Additionally, a reference WM image (such as calculated by anatomical image segmentation or by FA map estimated in the DW processing pipeline, to be discussed below) can be used as a reference to trim away voxels which may have large partial voluming. Thus, the first result of using 3dROIMaker is a labeled map (or set of maps, if sets of volumes are provided) of GM ROIs considered to form a FC network.

The second main output of 3dROIMaker is relevant for complementing the FC study with that of tractography. One would like to be able to find regions of WM which are related to each GM ROI and which provide physical connections between ROI pairs. The (probabilistic) tractography to be used to estimate these pathways is described below, but one basic requirement will be that the "target" ROIs input into the algorithm have some junction with WM voxels in order to search for intersecting fibers. Without such an interface it is difficult to commence or terminate tracts in regions of GM because the FA there is quite low (i.e., typically below tract propagation thresholds). Previous studies for producing targets have included inserting sizable spheres or uniformly inflating the ROI with the aim of reaching WM, both of which may severely overexpand into WM not associated with the GM. In 3dROIMaker ROI inflation is also employed; however, the expansion of an ROI is halted wherever it reaches WM labeled voxels in the reference image, reducing one likely category of errors.

Finally, standard Pearson correlation of mean time series between all pairs of the GM ROIs can be calculated using 3dNetCorr. For each network, a correlation matrix is returned, with the option to also return a matrix of associated Z-scores, as well. Such matrices are standard quantities of functional connectivity in networks.

DW processing

The goal for this line of processing is to resolve primary diffusion paths through WM, with an eye towards identifying the likely location of WM associated with the functionally-defined GM ROIs using DW data. The main mechanism for doing so is probabilistic tractography, which utilizes the uncertainty in the estimated DT ellipsoids and Monte Carlo simulations of wholebrain tractography to find likely WM voxels associated with individual and pairs of assigned targets [Parker et al., 2003; Behrens et al., 2003]. Again, the stages of processing are shown in Fig. 1.

Typically, the primary feature of preprocessing for DW images is volume registration, the attempted correction for eddy currents and sequence-induced distortions and the elimination of drop-out or error-dominated slices. Examples of existing software and pipelines for these aspects

include TORTOISE, RESTORE, FSL Diffusion Toolbox [Pierpaoli et al., 2010; Chang et al., 2005; Smith et al., 2004]. Realtime motion correction, performed during the acquisition of data, may also be used and offers advantages over post-processing corrections as seen in measured changes in ellipsoid parameter distributions, for example [Benner et al., 2011; Kober et al., 2012; Alhamud et al., 2012]. After preprocessing, the diffusion ellipsoids and parameters (particularly FA and $\mathbf{e}_1$ for tractography and MD, RD and L1 for statistical purposes) are easily calculated, with nonlinear fitting methods providing greater accuracy. These are available in most standard analysis packages (e.g., FSL-dtifit and AFNI's 3dDWItoDT were used here).

With tensors estimated, a useful first step in tractographic analysis is utilizing the deterministic method to visualize the data. 3dTrackID estimates tracts across the whole brain and between pairs of ROIs (using AND or OR logic). Tracts are generated using the FACTID (fiber assessment by continuous tracking including diagonals) algorithm, an improvement of the earlier FACT [Mori et al., 1999]. FACTID is a streamline algorithm that propagates tracts through each voxel along the local $\mathbf{e}_1$ orientation, but includes a test at edges and corners for continuing along a diagonal trajectory. The inclusion of this simple diagonal test has been shown to reduce sensitivity to noise and coordinate axes biases, without the need for data smoothing and while maintaining efficient propagation [Taylor et al., 2012]. Standard options for tract continuation can be selected: FA remaining above a certain threshold (e.g., >0.2), and angle between $\mathbf{e}_1$ in successive voxels being below a certain value (e.g., <60deg). Additionally, instead of an FA criterion, one may use a separately generated WM mask, such from segmentation of an anatomical image, to constrain tract propagation.

Basic statistics of the region though which numerical tracts pass are automatically calculated: mean and standard deviation of FA, MD, RD and L1, as well as mean length and numbers of tracts. The output tracts can be mapped to other coordinate spaces using map_TrackID, a procedure which can be useful for multisubject comparisons in standard space. Results are visualizable in 2D form, highlighting voxels through which tracts have passed, as well as in 3D projections using TrackVis [] or SUMA [Saad et al., 2004; Saad et al. 2012].

Due to the nature of MRI scanning, all parameter estimates have noise and errors incorporated into their final values. It is useful therefore to quantify confidence intervals of uncertainty, particularly for performing probabilistic tractography. The next subsections describe in detail the technical aspects of these procedures in FATCAT.

Uncertainty estimates with jackknife resampling

In the FACTID algorithm the main DT parameters of interest are FA and the first eigenvector, since these respectively determine the proxy location of WM and the orientation of propagating tracks. In particular, the vector $\mathbf{e}_1$ has two degrees of freedom for varying, so that two confidence intervals are required; its possible motion is accounted for by estimating how far it could move

along the mutually orthogonal $\mathbf{e}_2$ and $\mathbf{e}_3$ axes. In 3dDWUncert, the uncertainty estimates for FA and $\mathbf{e}_1$ are calculated using jackknife resampling [Efron, 1982], which is efficient both in terms of scan time and computation. Jackknife resampling works by analyzing subsets of a data set, from which it builds a theoretical pseudo-population (see below for more details). This method is broadly applicable to existing scan protocols and, importantly, does not require repeated acquisitions as, for example, the related bootstrap methods.

In order to obtain confidence estimates, Monte Carlo simulations have been used in conjunction with nonparametric resampling techniques (e.g., see [Pajevic & Basser, 2003]), such as the bootstrap [Davison & Hinkley, 1999; Jones, 2003] and direct variants [Chung et al., 2006; Whitcher et al., 2008]. In general, statistical resampling is used to investigate a given parameter of interest θ, by generating a distribution of estimates, θ^*_i, from which it is possible to calculate an estimator θ', as well as confidence intervals, standard errors, etc. In the case of the jackknife technique, this is done using randomly selected (without replacement) subsets of measures to calculate each θ^*_i. Therefore, from a single original data set, $Y=\{y_1, ..., y_M\}$, a (unordered) jackknife sample is created, $Y'=\{y'_1, ..., y'_{MJ}\}$, by omitting d values such that $M_J=M-d$, where d is typically much smaller than M. There are N_Y=binom(M, M_J) distinct subsets of variables, and the process is repeated a large number of times with the M_J values randomly selected at each iteration.

This process is illustrated schematically for diffusion data in Fig. 2. In the figure (1), M=12 is the number of initial DW measures, shown as gradient directions through an ellipsoid. From these, (1b) the non-resampled DT estimator, D', can be calculated, as well as estimators of associated parameters such as FA', $\mathbf{e}'_1$, etc. To perform jackknifing (2), N_J subsets of M_J =8 measures at a time are randomly selected (bold gradients). Then the DT of each jackknifed measure is estimated (3), from which distributions of parameter values of interest are calculated (4). In this case, the parameters are the FA and the difference between the jackknifed tensor's first eigenvector that that of the un-jackknifed samples, projected along both the latter's $\mathbf{e}_2$ and $\mathbf{e}_3$: mathematically, $\Delta\mathbf{e}^*_{1,2}=(\mathbf{e}'_1-\mathbf{e}^*_1)\cdot\mathbf{e}'_2$ and similarly for $\Delta\mathbf{e}^*_{1,3}$. Finally, the bias and confidence interval of the non-resampled DT estimators are obtained from the jackknifed parameter distributions (5).

The confidence intervals are strictly delimited by percentile locations of the distributions or, in the common case of Gaussian distributions, equivalently by known combinations of mean and standard deviation. In FATCAT, the latter, faster approach is used in the uncertainty estimates, as, at SNRs and M values of practical interest, jackknife distributions are well suited to Gaussian approximation. From Monte Carlo simulations of DW data including Rician noise, a ratio of subsample to sample size of $M_J/M\approx0.7$ generally yielded reasonable estimates of 95% confidence intervals for a large range of SNR and so is used in 3dDWUncert. It should be noted that 3dProbTrackID assumes a minimum amount of uncertainty in the tensor parameters: for $\mathbf{e}_1$, approx. 3deg toward either $\mathbf{e}_2$ or $\mathbf{e}_3$, and for FA, approx. 0.015.

Probabilistic tractography

With the combination of estimated DTI parameters, the uncertainty measures of 3dDWUncert and the tractography-ready maps of target ROIs from 3dROIMaker, probabilistic tractography can be performed. This is done using a large number of Monte Carlo iterations of wholebrain (deterministic) tractography estimations using FACTID. With each iteration, FA and $\mathbf{e}_1$ direction are perturbed at each voxel per the uncertainty estimates and whole brain tractography carried out. Locations of tracts which intersect any pairs of ROIs are recorded. For N_{MC} iterations with N_{seed} track seeds per voxel, locations are recorded where more than $f_{tr}N_{MC}N_{seed}$ tracks passed, where f_{tr} is a user-defined fractional threshold (tracks passing through individual ROIs are recorded separately, as well.). The set of all voxels connecting a pair of target (expanded GM) ROIs forms a WM ROI.

In several existing algorithms, probabilistic tractography is used to estimate the likelihood that a given target voxel is physically connected to each voxel in the brain, generally as a scaled value of the number of tracts connecting two locations. In FATCAT, however, the tractography results are structured for finding voxels which are likely in the WM connecting given target ROIs; the number of tracts through a voxel is used as an approximate gauge of the likelihood of including the voxel in the WM ROI. This latter interpretation avoids the difficulties of the former in trying to interpret the relative number of numerically reconstructed tracts as a proxy for some physiological "strength of structural connectivity," as well as question of how to compare relative strengths between ROIs of different sizes or subjects. Moreover, the WM ROIs themselves are useful outputs, whose structural properties may be probed using DTI quantities therein or mapping the ROIs to anatomical space for studying T1 or proton density values, for example. (It should be noted, though, that the number of tracks between ROIs is still recorded and output as informational value for the user.)

Statistics of DTI parameters per connective WM ROI are automatically calculated, similar to the 3dTrackID case above (i.e., mean and standard deviation of FA, track number, etc.). For a network of N_{ROI} GM ROIs, this results in a symmetric N_{ROI} x N_{ROI} matrix of values, whose i,jth values are the WM properties connecting ROIs i and j and whose diagonal values are for any tracks through each individual ROI. This matrix is the same size as a functional connectivity matrix derived for the same network of GM ROIs.

4. *EXAMPLE SUBJECT ANALYSIS AND RESULTS*

In this section, we provide an example case of combining RS-FMRI and DTI-tractography analyses using FATCAT. For comparison of tractography results, equivalent parts of the FSL-package Diffusion Toolbox software, dtifit, bedpostX and probtrackX (described below), were also run. We first describe the preprocessing steps for the data sets, the use of ICA with RS-

FMRI data to generate networks of ROIs for tractography, and conclude with the tractography results and comparisons.

Preprocessing

The data for this example was collected from a control subject as part of a larger study, with participants from the university campuses in Taipei. Participants were enrolled after providing written, informed consent. The study was approved by the local Ethics Committee and conducted in accordance with the Declaration of Helsinki.

Data is shown from one healthy subject (healthy control male, 24 years old). All MR images were carried out on a 3T Trio MR scanner (Siemens, Germany) equipped with a 32-channel phased-array head coil. A twice refocused spin-echo echo planar imaging (EPI) sequence was used for DWI acquisition. Three b=0 and 30 DW images with b = 1000 s/mm2 were acquired for each DWI set, with imaging parameters: TR=8800 ms, TE=101 ms, FOV= 24x24 cm, BW=1325 Hz/pixel and parallel acquisition (GRAPPA) with 2-fold acceleration. A T1-weighted MPRAGE scan was acquired with 256x256x192 voxels (1mm isotropic resolution). A resting state scan was acquired: 200 volumes (TR/TE=2500/30ms) with FOV=28.4x28.4cm using 3.4x3.4x3mm voxels.

Standard preprocessing steps were implemented using AFNI and FSL. Resting state data were processed following Biswal et al. (2010): first, motion correction with respect to the mean image was performed; time series from WM and cerebrospinal fluid (CSF) were regressed out, as well as size motion parameters (maximum motion in any direction was 0.83mm); spatial smoothing with a 6mm FWHM (full-width at half maximum) Gaussian blur was applied; the LFF range for temporal filtering was 0.01-0.1Hz; mean, linear and quadratic trends were removed; and the first five time points were removed to avoid pre-steady state signal. For the DWIs, we used FSL-eddy_correct, an affine registration (to the b=0 image) in order to correct for aspects of motion and gradient-induced distortions.

FMRI and DTI Analyses

After preprocessing, spatial ICA was performed in native functional space with FSL-melodic (http://fmrib.ox.ac.uk/analysis/research/melodic/), selecting decomposition into 20 ICs, a typical dimensionality in RS-FMRI studies. From the resulting components, four were chosen for tractography analysis because of their wide-brain coverage. The Z-score maps of these components were mapped to DW-native space using an affine transformation via the subject's T1-anatomical imageand are shown in Fig. 3 (thresholded at $Z>0$; left column of each panel). Network identifications were made by using 3dMatch in comparison with the 20 group ICs from the multicenter Functional Connectome Project (FCP) study [Biswal et al., 2010]. The IC-defined networks are shown in Fig. 3 (left columns of each panel), with the following

associations (i.e., all ICs here show significant but not identical overlap with the FCP networks, due for example, to different splitting of components): A) FCP 6, default mode network (DMN); B) FCP 20, containing the left and right (L-R) inferior and superior parietal lobules, middle temporal gyri and the medial and medial frontal gyri; C) FCP 11, the frontoparietal network; and D) FCP 17, the cingular gyrus, L-R superior frontal gyri and middle frontal gyri.

The Z-score maps were each converted to target ROIs for tractography using 3dROIMaker. Clusters were made by first thresholding values at Z>3 and volumes at voxels per cluster >130, and then inflating each ROI by two voxels but stopping expansion at an FA>0.2 WM skeleton. These final target ROIs for tractography are also shown in Fig. 3.

Fig. 4 shows and example of deterministic tractography results performed in DW-native space with 3dTrackID. The set of tracks running through any of the DMN network ROIs (targets shown in Fig. 3, panel A, second column) are shown using TrackVis. Colors denote local orientation along the tracks. Tracks are shown running along many expected pathways. However, since the deterministic tracts take no account of noise and parameter uncertainty, one can expect that the full, probabilistic tractography results would show more complete pathways among the ROIs. In the top panels of Fig. 5, voxels through which tracts passed (for networks A and C in Fig. 3) are shown in red, overlayed on the FA map; in the lower panels of the same figure, WM regions found between GM ROIs using probabilistic tractography (as described below) are shown for the respective networks. Significantly greater extents of WM are included in the latter set.

Two probabilistic tractographic analyses in DW-native space were run for comparison: the existing FSL software approach and the FATCAT method. In the former, first bedpostX is applied to model distributions of relevant parameter values per voxel using a Bayesian Monte Carlo approach [Behrens et al., 2007]; here, only one fiber direction per voxel was modeled (to match the current DTI-based approach of FATCAT). The probabilistic tractography program, probtrackX was then run separately on each network map of target ROIs, using standard stopping criteria and options: FA>0.2, angular deflection<60deg, 1 propagation direction per voxel, keeping tracts >15mm in length, 5000 iterations, integration step size 0.5mm (default). Using FATCAT, 3dDWUncert was first run for N_J=200 iterations, and example plots of the uncertainty for relevant parameters, in terms of bias and standard deviation estimated using jackknife resampling, are shown in Fig. 6. 3dProbTrackID was then run using criteria identical to what was used for probtrackX (except no step size is required) for all four networks simultaneously.

The results for each program are given in Fig. 7. WM ROIs found to connect pairs of target ROIs (orange) are shown in blue (3dProbTrackID) and in purple (probtrackX) for each network. The connectivity patterns produced by each program are broadly similar. Some regions of difference are highlighted with arrows: yellow for tracks appearing in only one set of results, and red for regions in which tracks may have been measured in both results but had very different

characteristics (e.g., a filled in volume vs filamentary structures). Qualitatively, the 3dProbTrackID WM regions tended to follow more circumscribed paths; for example, in panel A, the anterior-posterior running cingulate bundles are clear, while probtrackX included a much wider volume in the transcallosal region. 3dProbTrackID generally found connections between more ROIs. For example, a transcallosal tract between the posterior parietal lobules was found in B and anterior-posterior subcortical connections (identifiable as the inferior longitudinal fasciculus) in A were found with 3dProbTrackID but not using probtrackX.

An example of a set of matrices from associated functional and tractographic analyses is shown in Fig. 8. In the top row, functional matrices of correlation coefficients and Z-scores (zeroed along the diagonal) are shown, calculated between average time series in GM ROIs calculated using 3dROIMaker for Network A (the DMN; see Fig. 3). In the second and third rows, matrices of standard DTI parameters are shown, representing mean values in the track regions connecting GM ROIs as found by 3dProbTrackID. In the bottom row, measures of the number of voxels per WM region and the track count during the probabilistic tractography iterations are given. It should be noted that since not all target regions were found to be connected (to be expected), the structural matrices contain empty cells.

5. DISCUSSION AND CONCLUSIONS

We have described a basic set of tools for assisting in two types of MRI analysis: functional MRI and diffusion-based tractography. These methods produce several quantitative measures which can be used in describing complementary features of the brain as recently highlighted in a recent review [Johansen-Berg, 2011]. Though no single "correct" way for doing so is obvious for lack of ground truths, the software in FATCAT has been designed to assist in this process: simplifying the process of calculating several features of both functional and structural connectivity while remaining flexible to types of processing and analysis.

The capabilities and procedures for implementing FMRI and DTI-based tractographic analysis using FATCAT were presented in an example case. Target ROIs for tractography were generated directly from a subject's RS-FMRI data, with 3dROIMaker using anatomical information for determining likely intersections of the functional GM ROIs with nearby WM. Probabilistic tractography results of structural connectivity with 3dDWUncert and 3dProbTrackID were broadly comparable to those of existing FSL programs, in terms of connected GM ROIs and path regions. In the absence of a gold standard, it is difficult to judge which of the two approaches produces more valid results. Qualitatively, 3dProbTrackID results were more spatially circumscribed within white matter with more physiologically identifiable paths produced between several ROI pairs.

A striking feature of the FATCAT programs is their relative execution speed. While many programs for probabilistic tractography (including those tested here using FSL) can run for more

than a day for uncertainty estimations and tracking within a single network, 3dDWUncert and 3dProbTrackID completed execution in approximately 7min and 25min, respectively, on the same hardware[1] and for four rather than one network. One of the reasons for this sizable decrease in runtime is the efficiency of the algorithms in each: uncertainty estimations use jackknife resampling of DTI data and utilizing the Gaussian interval approximation; the tract propagation algorithm in FACTID is also efficient. Whole brain tractography using 3dTrackID on a 128x128x70 voxels (2mm isotropic) dataset took <4secs on the same machine. Even with more complex diffusion models per voxel such as Qball, the tracking execution speed is not expected to increase significantly. Moreover, testing for connectivity among several networks simultaneously adds very little computational time, which is of great use in multi-component RSN studies.

White matter bundles can cross, "kiss" and fan out in complicated structures at spatial scales considerably finer than voxel sizes on the order of millimeters. Such complex patterns are better (though by no means fully) captured with high order diffusion models which model more than one direction per voxel. At this stage, FATCAT only supports DTI modeling and single direction-per-voxel tractography. Work is currently underway to add multi-direction support using Q-ball modeling in an efficient manner. We are also considering improvements to the methods of defining target ROIs for tractography from functional data. One improvement may consist of using cortical surface models to inform ROI expansion [Greenberg et al., 2012].

As with most neuroimaging analysis tools, further tests of validity will be required, particularly when including higher order improvements to the methods. Such verification has traditionally been difficult in tractography, given a lack of gold standard tests; even histological data is generally insufficient for examining fine white matter structures in the brain. A well-known test phantom model exists for analysis [Poupon et al., 2008; Fillard et al., 2011], and the FACTID tracking algorithm used in FATCAT has been tested on this, as well as on both in vivo and vivo+simulation data sets [Taylor et al., 2012]. However, while quite useful, the phantom cannot match size, scale and complexity of brain architecture. Similarly, many in vivo tests to date can only be used to verify algorithm behavior through major fiber bundle pathways but not necessarily in finer structures or in crossing/kissing fiber regions. It is possible that neuroanatomical tracing methods [e.g., Dyrby et al., 2007; Schmahmann et al., 2007] may be improved and expanded to study human data sets for greater validation of in vivo tractography. Such evaluations would be useful for continuing to assess tractography algorithms.

In conclusion, FATCAT is a set of publicly available software tools for combining several aspects of functional and tractographic MRI analysis towards a better understanding of brain function. The tools are integrable with many pre- and post-processing pipelines in standard analysis packages. They are also run from terminal command lines, simplifying group processing, and

[1] MacBook Pro, Mac OS X, single processor 2.3 GHz and 4GB RAM.

produce easily viewable outputs for guiding analysis. FATCAT programs and demo data are freely available and distributed with the AFNI/SUMA suite (http://afni.nimh.nih.gov) and users are encouraged to use AFNI's message board for support and feedback.

ACKNOWLEDGMENTS
The authors would like to thank Ching-Po Lin for the use of test subject data for this work, and Suril Gohel and Bharat Biswal for analysis advice concerning various toolbox components. This research was supported in part by the NIMH and NINDS Intramural Research Programs of the NIH and in part by NIH grant R01 AG032088.

REFERENCES

Alhamud A, Tisdall MD, Hess AT, Hasan KM, Meintjes EM, van der Kouwe AJW. 2012. Volumetric Navigators for Real-Time Motion Correction in Diffusion Tensor Imaging. Magn Reson Med 68:1097-1108.

Anderson AW. 2005. Measurement of fiber orientation distributions using high angular resolution diffusion imaging. Magn Reson Med 54:1194-1206.

Basser PJ, Mattiello J, LeBihan D. 1994. MR diffusion tensor spectroscopy and imaging. Biophys J 66:259–67.

Basser PJ. 1995. Inferring microstructural features and the physiological state of tissues from diffusion-weighted images. NMR Biomed 8:333–44.

Basser PJ, Pajevic S, Pierpaoli C, Duda J, Aldroubi A. 2000. In vivo tractography using DT-MRI data. Magn Reson Med 44:625–32.

Beckmann CF, DeLuca M, Devlin JT, Smith SM. 2005. Investigations into resting-state connectivity using independent component analysis. Philos Trans R Soc Lond B Biol Sci 360: 1001–1013.

Behrens TEJ, Woolrich MW, Jenkinson M, Johansen-Berg H, Nunes RG, Clare S, Mathews PM, Brady JM, Smith SM. 2003. Characterization and propagation of uncertainty in diffusion-weighted MR imaging. Magn Reson Med 50:1077–88.

Behrens TEJ, Johansen-Berg H, Jbabdi S, Rushworth MFS, Woolrich MW. 2007. Probabilistic diffusion tractography with multiple fibre orientations: What can we gain? NeuroImage 34:144-55.

Benner T, van der Kouwe AJW, Sorensen AG. 2011. Diffusion imaging with prospective motion correction and reacquisition. Magn Reson Med 66:154–167.

Biswal B, Yetkin FZ, Haughton VM, Hyde JS. 1995. Functional connectivity in the motor cortex of resting human brain using echo-planar MRI. Magn Reson Med 34:537–541.

Biswal BB, Mennes M, Zuo XN, Gohel S, Kelly C, Smith SM, Beckmann CF, Adelstein JS, Buckner RL, Colcombe S, Dogonowski AM, Ernst M, Fair D, Hampson M, Hoptman MJ, Hyde JS, Kiviniemi VJ, Kötter R, Li SJ, Lin CP, Lowe MJ, Mackay C, Madden DJ, Madsen KH, Margulies DS, Mayberg HS, McMahon K, Monk CS, Mostofsky SH, Nagel BJ, Pekar JJ, Peltier SJ, Petersen SE, Riedl V, Rombouts SA, Rypma B, Schlaggar BL, Schmidt S, Seidler RD, Siegle

GJ, Sorg C, Teng GJ, Veijola J, Villringer A, Walter M, Wang L,Weng XC, Whitfield-Gabrieli S, Williamson P, Windischberger C, Zang YF, Zhang HY, Castellanos FX, Milham MP. 2010. Toward discovery science of human brain function. Proc Natl Acad Sci U S A 107:4734–4739.

Bonner M, Peelle JE, Cook PA, Grossman M. 2013. Heteromodal conceptual processing in the angular gyrus. NeuroImage 71:175-186.

Calhoun VD, Pekar JJ, McGinty VB, Adali T, Watson TD, Pearlson GD. 2002. Different activation dynamics in multiple neural systems during simulated driving. Hum Brain Mapp 16:158–167.

Catani M, Howard RJ, Pajevic S, Jones DK. 2002. Virtual in vivo interactive dissection of white matter fasciculi in the human brain. NeuroImage 17:77–94.

Chang LC, Jones DK, Pierpaoli C. 2005. RESTORE: robust estimation of tensors by outlier rejection. Magn Reson Med 53(5):1088-95.

Chen G, Glen DR, Saad ZS, Hamilton JP, Thomason ME, Gotlib IH, Cox RW. 2011. Vector autoregression, structural equation modeling, and their synthesis in neuroimaging data analysis. Comput Biol Med 41(12):1142-1155.

Chung SW, Lu Y, Henry RG. 2006. Comparison of bootstrap approaches for estimation of uncertainties of DTI parameters. NeuroImage 33:531-541.

Conturo TE, Lori NF, Cull TS, Akbudak E, Snyder AZ, Shimony JS, McKinstry RC, Burton H, Raichle ME. 1999. Tracking neuronal fiber pathways in the living human brain. Proc Natl Acad Sci USA 96:10422–10427.

Cox RW. 1996. AFNI: software for analysis and visualization of functional magnetic resonance neuroimages. Comput Biomed Res 29:162–173.

Damoiseaux JS, Rombouts SA, Barkhof F, Scheltens P, Stam CJ, Smith SM, Beckmann CF. 2006. Consistent resting-state networks across healthy subjects. Proc Natl Acad Sci USA 103:13848–13853.

Davison AC, Hinkley DV. 1999. Bootstrap methods and their application. Cambridge, UK: Cambridge University Press.

Dice L. 1945. Measures of the amount of ecologic association between species. Ecology 26:207–302.

Dyrby TB, Sogaard LV, Parker GJ, Alexander DC, Lind NM, Baare WF, Hay-Schmidt A, Eriksen N, Pakkenberg B, Paulson OB, Jelsing J. 2007. Validation of in vitro probabilistic tractography. Neuroimage 37, 1267–1277.

Friston KJ, Buchel C, Fink GR, Morris J, Rolls E, Dolan R. 1997. Psychophysiological and modulatory interactions in neuroimaging. NeuroImage 6:218-229.

Efron B. 1982. The Jackknife, the Bootstrap and Other Resampling Plans. CBMS-NSF Regional Conference Series in Applied Mathematics Monograph 38, SIAM, Philadelpia.

Fillard P, Descoteaux M, Goh A, Gouttard S, Jeurissen B, Malcolm J, Ramirez-Manzanares A, Reisert M, Sakaie K, Tensaouti F, Yo T, Mangin J-F, Poupon C. 2011. Quantitative evaluation of 10 tractography algorithms on a realistic diffusion MR phantom. Neuroimage 1;56(1):220-34.

Friston KJ, Harrison L, Penny W. 2003. Dynamic causal modelling. NeuroImage 19(4):1273-302.

Goebel R, Roebroeck A, Kim DS, Formisano E. 2003. Investigating directed cortical interactions in time-resolved fMRI data using vector autoregressive modeling and Granger causality mapping. Magn Reson Imaging 21:1251-1261.

Greenberg AS, Verstynen T, Chiu YC, Yantis S, Schneider W, Behrmann M. 2012. Visuotopic cortical connectivity underlying attention revealed with white-matter tractography. J Neurosci 32(8):2773-82.

Groppe DM, Makeig S, Kutasc M. 2009. Identifying reliable independent components via split-half comparisons. Neuroimage 45(4):1199–1211.

Hagmann P, Thiran JP, Jonasson L, Vandergheynst P, Clarke S, Maeder P, Meuli R. 2003. DTI mapping of human brain connectivity: statistical fibre tracking and virtual dissection. NeuroImage 19:545–54.

He Y, Wang L, Zang Y, Tian L, Zhang X, Li K, Jiang T. 2007. Regional coherence changes in the early stages of Alzheimer's disease: a combined structural and resting-state functional MRI study. Neuroimage 35(2):488-500.

Huettel SA, Song AW, McCarthy G. 2009. Functional Magnetic Resonance Imaging (2nd ed.). Massachusetts: Sinauer.

Jones, DK. 2003. Determining and visualizing uncertainty in estimates of fiber orientation from diffusion tensor MRI. Magn Reson Med 49:7-12.

Kannurpatti SS, Biswal BB. 2008. Detection and scaling of task induced fMRI-BOLD response using resting state fluctuations. Neuroimage 40:1567–1574.

Kendall MG, Babington Smith B. 1939. The Problem of m Rankings. The Annals of Mathematical Statistics 10(3):275–287.

Kingsley PB. 2006. Introduction to Diffusion Tensor Imaging Mathematics: Part I. Tensors, Rotations, and Eigenvectors. Concepts Magn Reson 28A:101-122.

Kiviniemi V, Kantola JH, Jauhiainen J, Tervonen O. 2004. Comparison of methods for detecting nondeterministic BOLD fluctuation in fMRI. Magn Reson Imaging 22:197–203.

Kober T, Gruetter R, Krueger G. 2012. Prospective and retrospective motion correction in diffusion magnetic resonance imaging of the human brain. NeuroImage 59:389–398.

Kwong KK, Belliveau JW, Chesler DA, Goldberg IE, Weisskoff RM, Poncelet BP, Kennedy DN, Hoppel BE, Cohen MS, Turner R. 1992. Dynamic magnetic resonance imaging of human brain activity during primary sensory stimulation. Proc. Natl. Acad. Sci. USA 89:5675–5679.

Lazar M, Weinstein DM, Tsuruda JS, Hasan KM, Arfanakis K, Meyerand ME, Badie B, Rowley HA, Haughton V, Field A, Alexander AL. 2003. White matter tractography using diffusion tensor deflection. Hum Brain Mapp 18, 306-321.

Le Bihan D. 1995. Molecular diffusion, tissue microdynamics and microstructure. NMR Biomed 8:375-86.

Le Bihan D, Johansen-Berg H. 2012. Diffusion MRI at 25: Exploring brain tissue structure and function. NeuroImage 61:324-341.

Lowe MJ, Mock BJ, Sorenson JA. 1998. Functional connectivity in single and multislice echoplanar imaging using resting state fluctuations. Neuroimage 7:119–132.

McIntosh AR, Gonzalez-Lima F. 1994. Structural equation modeling and its application to network analysis in functional brain imaging. Hum Brain Mapp 2:2–22.

McKeown MJ, Jung TP, Makeig S, Brown G, Kindermann SS, Lee TW, Sejnowski TJ. 1998. Spatially independent activity patterns in functional MRI data during the stroop color-naming task. Proc Natl Acad Sci U S A 95:803–810.

Mori S, Crain BJ, Chacko VP, van Zijl PC. 1999. Three dimensional tracking of axonal

projections in the brain by magnetic resonance imaging. Ann Neurol 45:265–9.

Ogawa S, Lee TM, Kay AR, Tank DW. 1990. Brain magnetic resonance imaging with contrast dependent on blood oxygenation. Proc Natl Acad Sci USA 87: 9868–9872.

Özarslan E, Shepherd TM, Vemuri BC, Blackband SJ, Mareci TH. 2006. Resolution of complex tissue microarchitecture using the diffusion orientation transform (DOT). NeuroImage 31:1086-1103.

Pajevic S, Basser PJ. 2003. Parametric and non-parametric statistical analysis of DT-MRI data. J Magn Reson 161(1):1-14.

Parker GJ, Haroon HA, Wheeler-Kingshott CA. 2003. A framework for a streamline-based probabilistic index of connectivity (PICo) using a structural interpretation of MRI diffusion measurements. J Magn Reson Imaging 18(2):242-54.

Pierpaoli C, Walker L, Irfanoglu MO, Barnett A, Basser P, Chang L-C, Koay C, Pajevic S, Rohde G, Sarlls J, Wu M. 2010. TORTOISE: an integrated software package for processing of diffusion MRI data, ISMRM 18th annual meeting, Stockholm, Sweden, #1597.

Poupon C, Rieul B, Kezele I, Perrin M, Poupon F, Mangin J-F. 2008. New diffusion phantoms dedicated to the study and validation of high-angular-resolution diffusion imaging (HARDI) models. Magn Reson Med 60(6):1276–83.

Raichle ME, MacLeod AM, Snyder AZ, Powers WJ, Gusnard DA, Shulman GL. 2001. A default mode of brain function. Proc Natl Acad Sci U S A 98:676–682.

Saad ZS, Reynolds RC, Argall B, Japee S, Cox RW. 2004. SUMA: an interface for surface-based intra- and inter-subject analysis with AFNI. 2004 IEEE International Symposium on Biomedical Imaging: From Nano to Macro. IEEE, Arlington, VA, pp. 1510–1513.

Saad ZS, Reynolds RC. 2012. Suma. Neuroimage 62(2):768-73.

Sbadbi S, Johansen-Berg H. 2011. Tractography: Where Do We Go from Here? Brain Connectivity 1(3):169.

Schmahmann JD, Pandya DN, Wang R, Dai G, D'Arceuil HE, De Crespigny AJ, Wedeen VJ. 2007. Association fibre pathways of the brain: parallel observations from diffusion spectrum imaging and autoradiography. Brain 130, 630–653.

Seeley WW, Menon V, Schatzberg AF, Keller J, Glover GH, Kenna H, Reiss AL, Greicius MD.

2007. Dissociable intrinsic connectivity networks for salience processing and executive control. J Neurosci 27:2349–2356.

Simonyan K, Ludlow CL. 2012. Abnormal structure-function relationship in spasmodic dysphonia. Cereb Cortex 22(2):417-25.

Smith S, Jenkinson M, Woolrich M, Beckmann C, Behrens T, Johansen-Berg H, Bannister P, De Luca M, Drobnjak I, Flitney D, Niazy R, Saunders J, Vickers J, Zhang Y, De Stefano N, Brady J, Matthews P. 2004. Advances in functional and structural MR image analysis and implementation as FSL. NeuroImage 23:208–219.

Smith JF, Pillai A, Chen K, Horwitz B. 2011. Effective Connectivity Modeling for fMRI: Six Issues and Possible Solutions Using Linear Dynamic Systems. Front Syst Neurosci 5:104.

Staempfli P, Reischauer C, Jaermann T, Valavanis A, Kollias S, Boesiger P. 2008. Combining fMRI and DTI: a framework for exploring the limits of fMRI-guided DTI fiber tracking and for verifying DTI-based fiber tractography results. NeuroImage 39(1):119-126.

Taylor PA, Cho KH, Lin CP, Biswal BB. 2012. Improving DTI tractography by including diagonal tract propagation. PLoS One 7(9):e43415.

Tuch DS, Reese TG, Wiegell MR, Makris N, Belliveau JW, Wedeen VJ. 2002. High angular resolution diffusion imaging reveals intravoxel white matter fiber heterogeneity. Magn Reson Med 48:577-582.

Tuch DS. 2004. Q-ball imaging. Magn Reson Med 52:1358-1372.

Wang R, Benner T, Sorensen AG, Wedeen VJ. 2007. Diffusion Toolkit: A Software Package for Diffusion Imaging Data Processing and Tractography. Proc Intl Soc Mag Reson Med 15:3720.

Wedeen VJ, Hagmann P, Tseng WI, Reese TG, Weisskoff RM. 2005. Mapping complex tissue architecture with diffusion spectrum magnetic resonance imaging. Magn Reson Med 54:1377-1386.

Weinstein DM, Kindlmann GL, Lundberg EC. 1999. Tensorlines: advection-diffusion based propagation through diffusion tensor fields, in: IEEE Visualization Proceedings, San Francisco pp. 249–253.

Westin CF, Maier SE, Khidir B, Everett P, Jolesz FA, Kikinis R. 1999. Image processing for diffusion tensor magnetic resonance imaging. In Taylor, C., Colchester, A. (Eds.), Lecture Notes in Computer Science: Medical Image Computing and Computed-Assisted Intervention. Springer-

Verlag, Cambridge, pp. 441–452.

Whitcher B, Tuch DS, Wisco JJ, Sorensen AG, Wang L. 2008. Using the Wild Bootstrap to Quantify Uncertainty in Diffusion Tensor Imaging. Hum Brain Mapp 29:346-362.

Xiong J, Parsons LM, Gao JH, Fox PT. 1999. Interregional connectivity to primary motor cortex revealed using MRI resting state images. Hum Brain Mapp 8:151–156.

Zang Y, Jiang T, Lu Y, He Y, Tian L. 2004. Regional homogeneity approach to fMRI data analysis. Neuroimage 22(1):394-400.

Zang YF, He Y, Zhu CZ, Cao QJ, Sui MQ, Liang M, Tian LX, Jiang TZ, Wang YF. 2007. Altered baseline brain activity in children with ADHD revealed by resting-state functional MRI. Brain Dev 29:83–91.

Zou QH, Zhu CZ, Yang Y, Zuo XN, Long XY, Cao QJ, Wang YF, Zang YF. 2008. An improved approach to detection of amplitude of low-frequency fluctuation (ALFF) for resting-state fMRI: fractional ALFF. J Neurosci Methods 172:137–141.

FIGURES and CAPTIONS

FIGURE 1: Schematic of a set of stages of combined FMRI (dark gray boxes) and DTI-tractography (light gray boxes) analyses, highlighting the possible use of FATCAT programs (bold, blue) and showing additional steps in available software (italics).

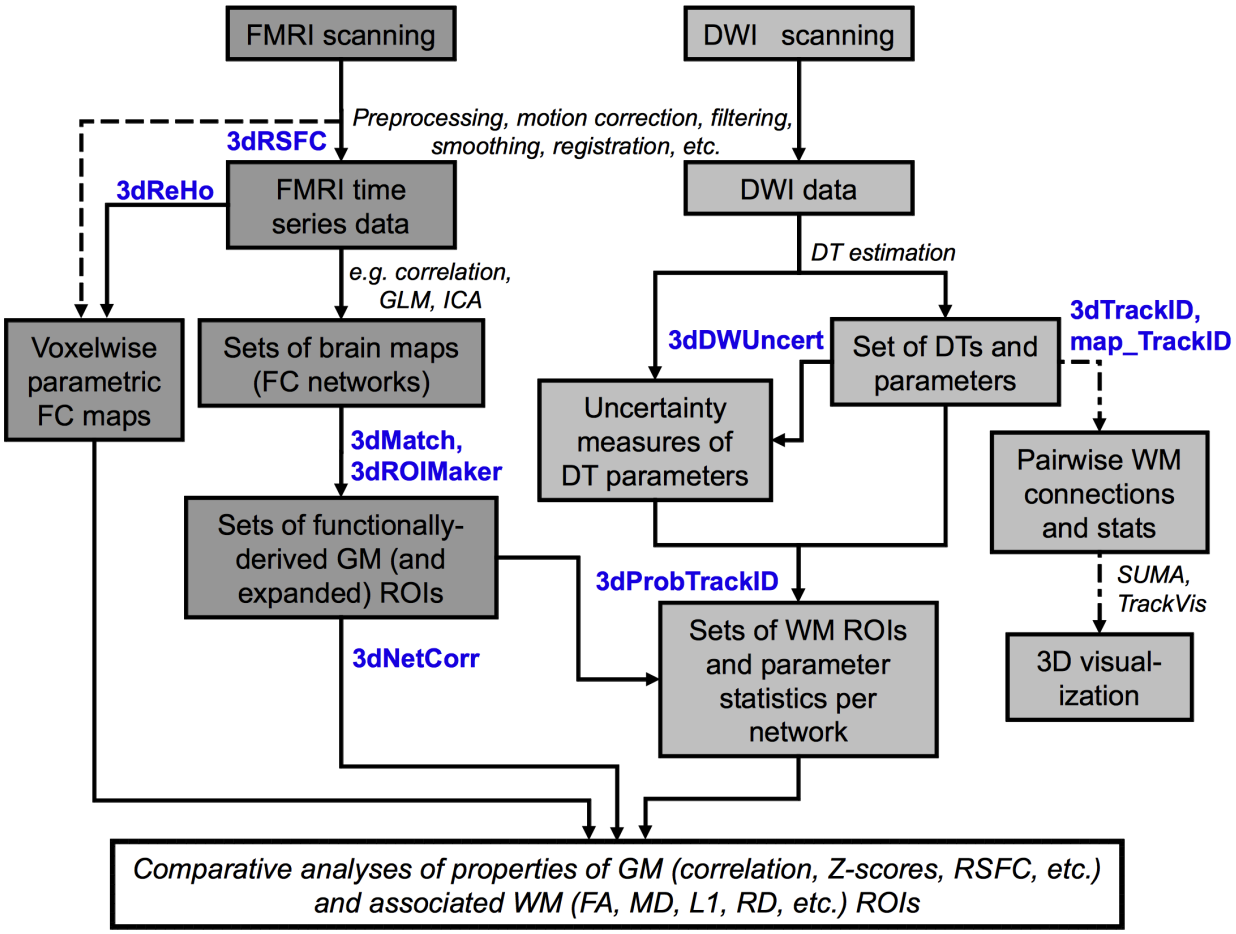

FIGURE 2: Representation (2D with M=12) of estimating DTI parameter confidence intervals using the jackknife resampling technique. (1) Initial DW measures are obtained, from which (1b) full estimates of the DT and associated parameters are made. For the jackknife process, (2) a random subset of $M_J<M$ measures are selected, from which (3) a sample tensor D* is calculated, as well as (4) its associated parameters. Steps (2-4) are repeated a large number N_J times to create a jackknifed pseudopopulation for each parameter, from which (5) percentile ranges can be found directly from ordering the data set, or from using a Gaussian approximation of the distribution. The latter method is applicable to DTI results and implemented in FATCAT for the sake of efficiency.

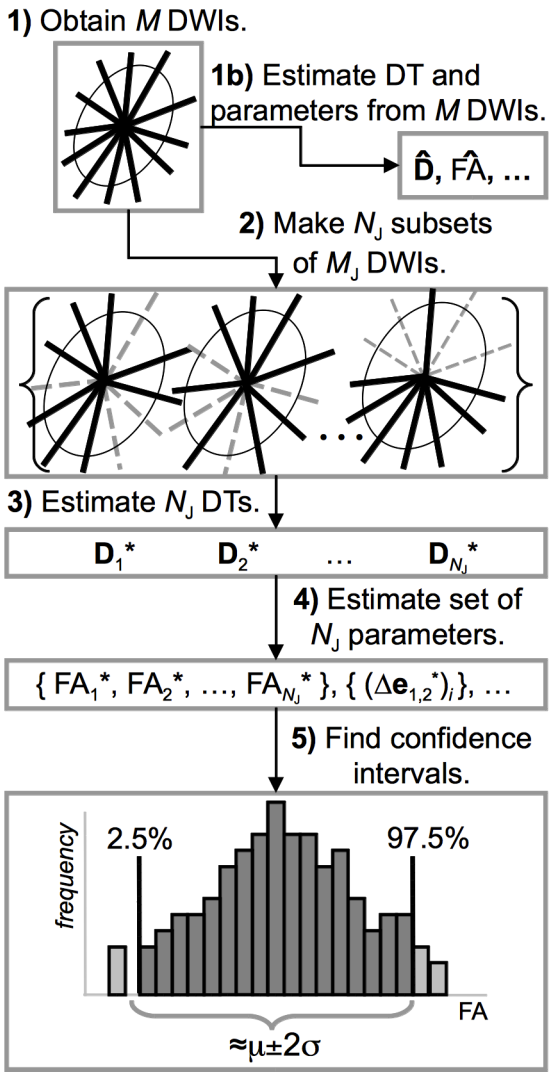

FIGURE 3: Four components from ICA of RS-FMRI time series overlaid on a T1-weighted anatomical mapped to DWI space. Z-score maps of each IC are shown (left column of each panel) with images thresholded at Z>0. Also shown are corresponding, inflated ROIs created using 3dROIMaker (colors independent per panel). Initial clusters were thresholded to have >130 voxels, and inflation was stopped at a WM skeleton defined to be wherever FA>0.2.

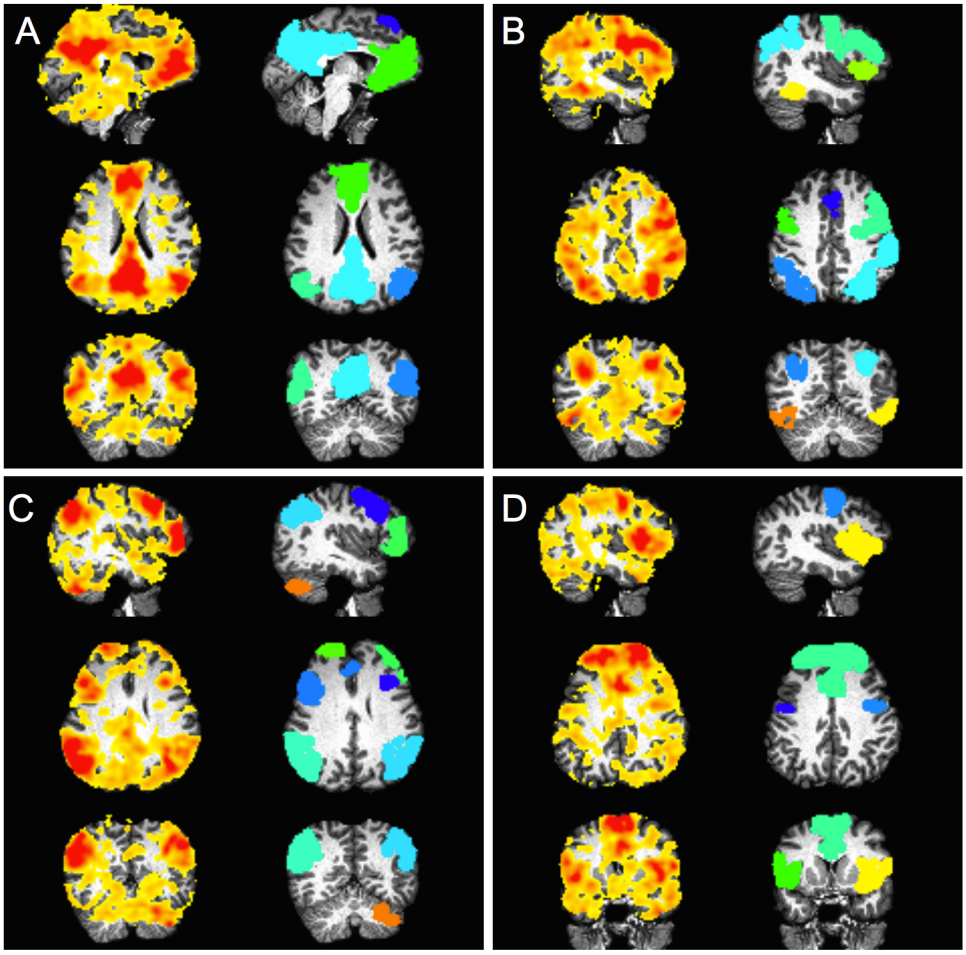

FIGURE 4: Deterministic tractography results using 3dTrackID with target ROIs shown in Fig. 3A. Tracks are displayed using TrackVis, with a T1 image (mapped to DW-native space) as background. In the top row tracks through any target ROI (OR logic) are shown, and in the bottom row only tracks passing through pairs of ROIs (pairwise AND logic) are shown.

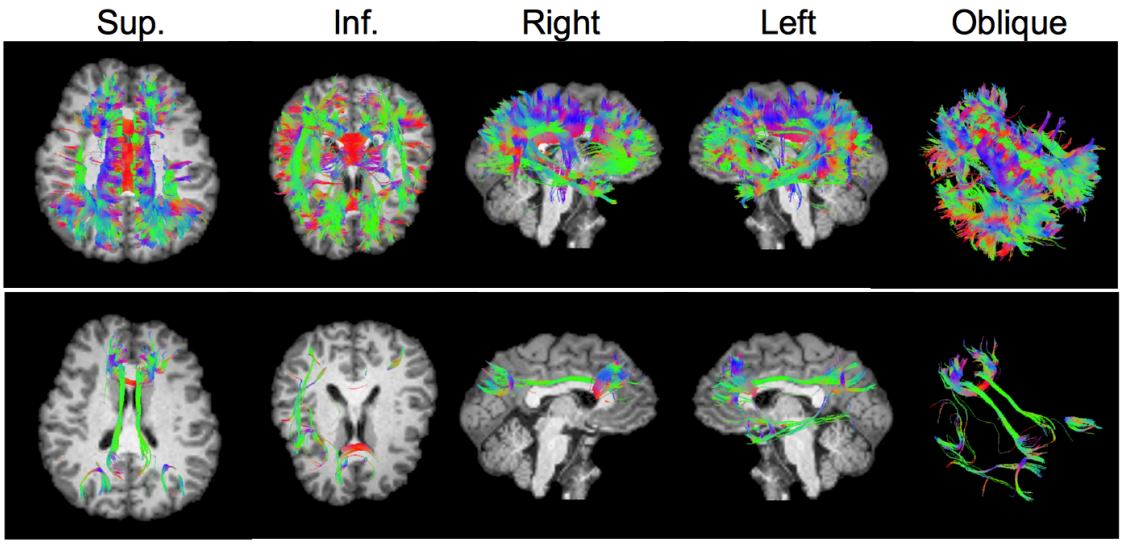

FIGURE 5: A comparison of WM regions connecting GM ROIs using deterministic (top panels) and probabilistic (bottom panels) tractography for networks A and C (shown in Fig. 3). Approximate locations of GM ROIs are shown with yellow dashes. The deterministic results are a subset of the probabilistic results (here, unthresholded), which shows significantly greater numbers and volumes of WM. Images are in DW-native space.

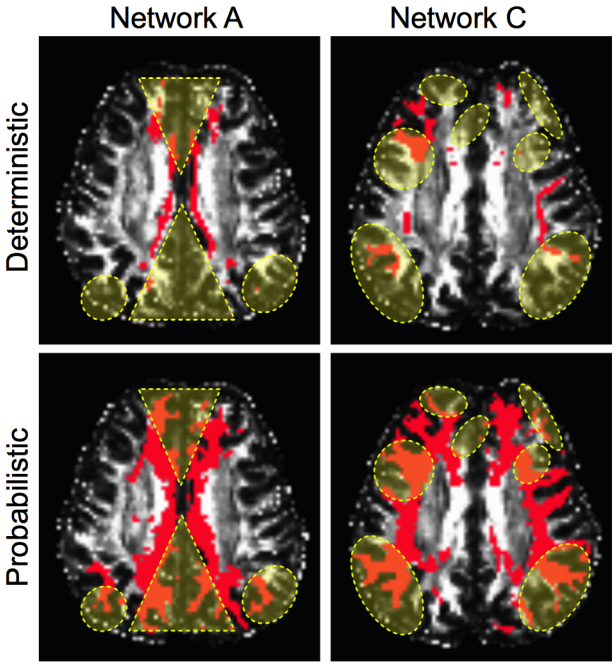

FIGURE 6: Examples of uncertainty values across brain slices, as estimated with jackknife resampling using 3dDWUncert. Distinct differences in GM and WM are evident, as well as the qualitative difference in first eigenvector uncertainty along the different degrees of freedom.

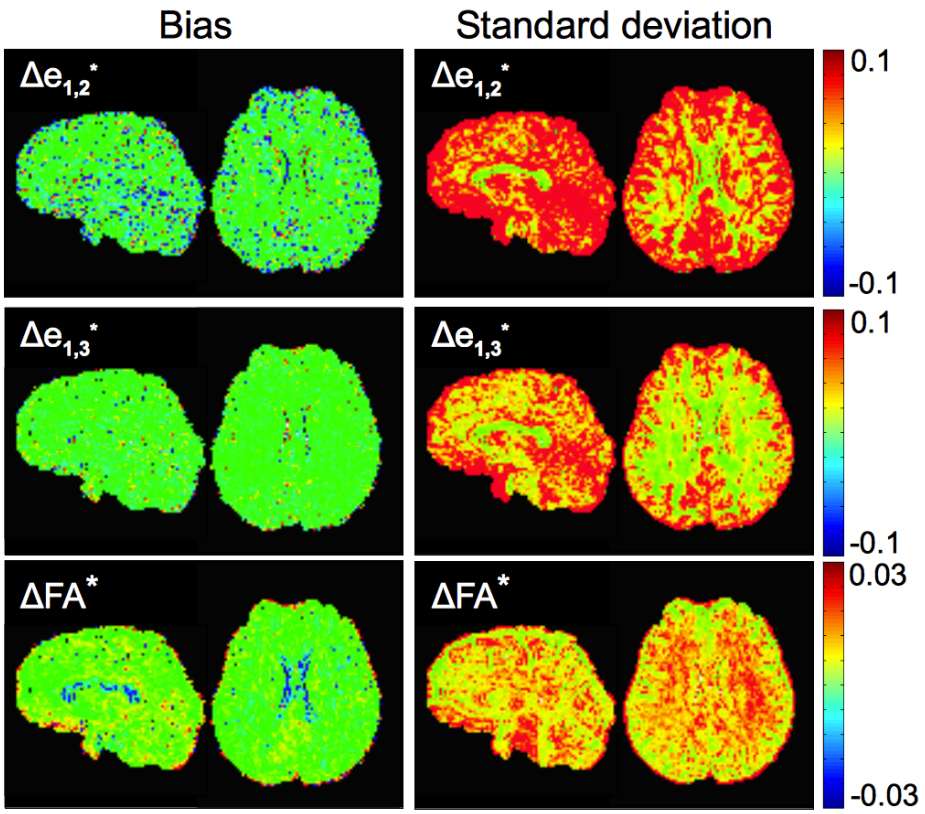

FIGURE 7: A comparison of probabilistic tractography results for 3dDWUncert+3dProbTrackID (blue) and FSL's bedpostX+probtrackX (purple). Networks of ROIs (orange) were made using ICA of RS-FMRI data, thresholding results at Z=3.0 and then inflating the GM ROIs using 3dROIMaker (see Fig. 3 and text for details). Similar tracking options were used for both programs (FA>0.2, angular deflection<60deg, 1 propagation direction per voxel, 5000 iterations). Tracking results show broadly similar connectivity, with generally more circumscribed WM track regions found by 3dProbTrackID, wich also tended to find connections between more ROIs. Tracking was performed in DW-native space, in which images are shown.

(figure on next page)

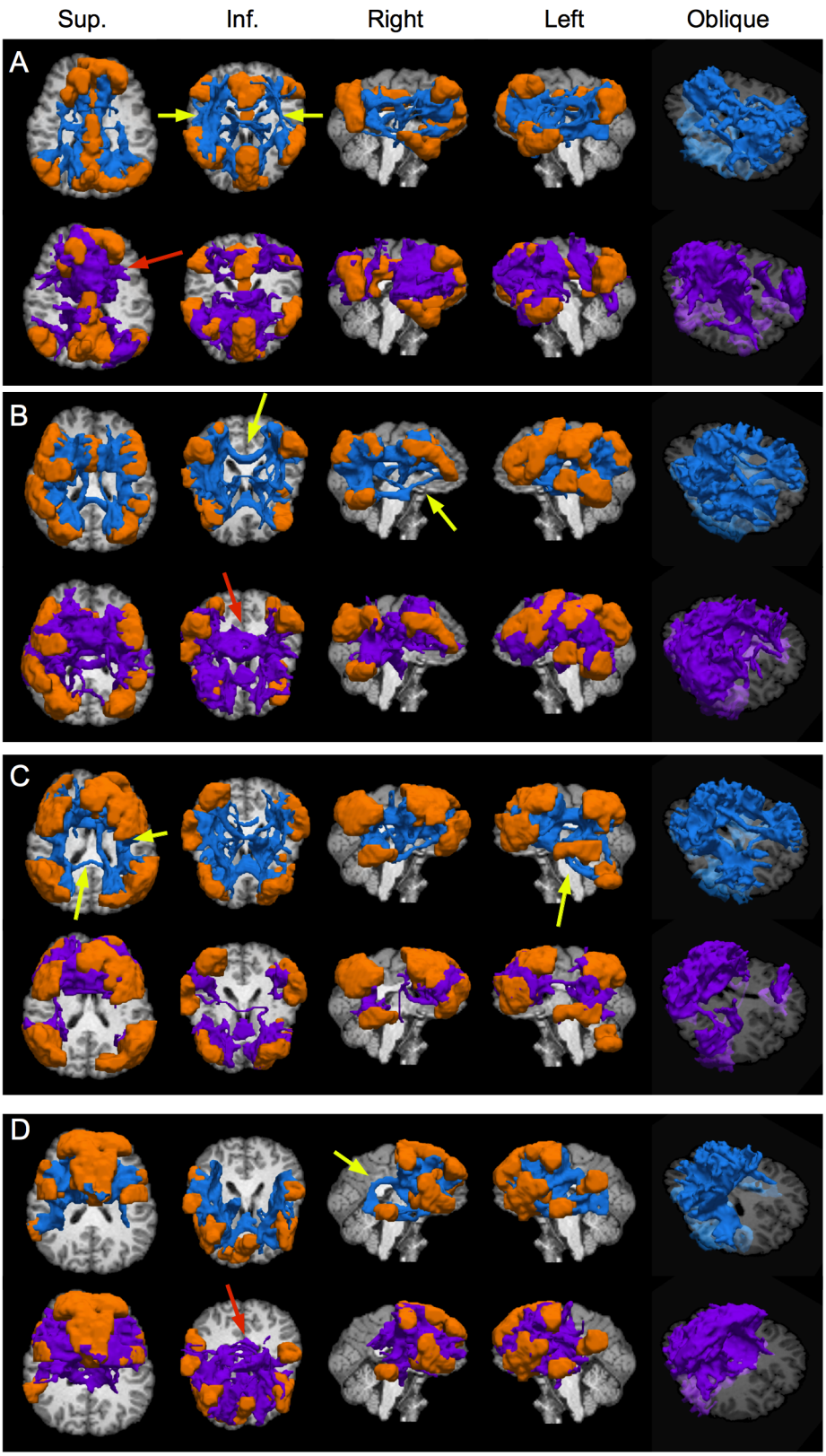
Sup.
Inf.
Right
Left
Oblique
A
B
C
D

FIGURE 8: An example set of matrices of functional and structural analyses for network A (the DMN; see Fig. 3), as determined using 3dProbTrackID. In the top row are correlation matrices of average time series of GM ROIs in the network (ROI labels have been ignored in this example). In the middle rows, standard DTI parameters are given, representing the mean values in the WM regions connecting the targets. Finally, the number of voxels in the final WM regions and the number of tracts found during the probabilistic tractography are given in the fourth row.